Energy & Environmental Science

Accepted Manuscript

This article can be cited before page numbers have been issued, to do this please use: F. Mo, G. Liang, Q. Meng, Z. Liu, H. Li, J. Fan and C. Zhi, *Energy Environ. Sci.*, 2019, DOI: 10.1039/C8EE02892C.

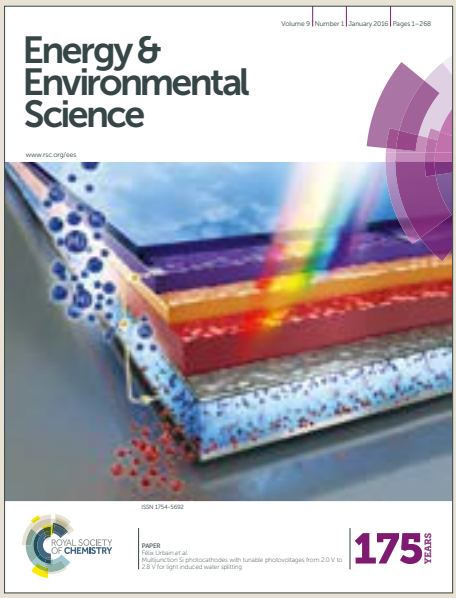

ROYAL SOCIETY OF CHEMISTRY

rsc.li/ees

View Article Online
DOI: 10.1039/C8EE02892C

Journal Name

ARTICLE

A flexible rechargeable aqueous zinc manganese-dioxide battery working at -20 °C

Received 00th January 20xx,
Accepted 00th January 20xx

DOI: 10.1039/x0xx00000x

www.rsc.org/

Funian Mo,[†a] Guojin Liang,[†a] Qiangqiang Meng,[a, b] Zhuoxin Liu,[a] Hongfei Li,[a] Jun Fan*,[a] and Chunyi Zhi*[a,c]

It remains a challenge to render the aqueous batteries operating at subzero temperatures properly, not even to mention the maintenance of their flexibility and mechanical robustness. This fundamentally arises from the freezing of hydrogel electrolytes under such low temperature, resulting in performance deterioration and elasticity loss. Here we propose an intrinsically freeze-resistant flexible zinc manganese-dioxide battery (Zn-MnO_2-B) comprising a designed anti-freezing hydrogel electrolyte which can preclude the ice crystallization of the hydrogel component and maintain a high ion conductivity even at -20 °C. Benefiting from the exceptional freeze resistance, the fabricated anti-freezing Zn-MnO_2-B (AF-battery) exhibits excellent electrochemical stability and mechanical durability at subzero temperatures. Even at -20 °C, the specific capacity of AF-battery can be retained over 80% with Coulombic efficiencies approaching ~100%, compared to the thorough performance failure of the Zn-MnO_2-B with traditional polyacrylamide (PAM) hydrogel electrolyte. More impressively, the flexibility of batteries can also be well maintained even under severe mechanical stresses at subzero temperatures, such as being bent, compressed, hammered or washed in ice bath. Furthermore, the AF-battery sealed in ice cube can be integrated in series to power a wristband of electronic watch, LED lights and a 72 cm^2 electroluminescent panel. It is believed that this work opens new perspectives to develop anti-freezing batteries and would role as a model system for developing new hydrogel aqueous electrolyte for flexible batteries in the extremely cold environment.

Introduction

Benefitting from the intrinsic safety, eco-friendliness and flexibility, aqueous batteries based on hydrogel electrolyte are particularly advantageous for energy storage in flexible electronics.[1-6] However, due to the water molecules existing in polymer networks, conventional hydrogel electrolytes inevitably freeze and lose elasticity at subzero temperatures, which severely affects their electrochemical performance and practical applications in extremely cold environment.[7] Existing strategies used for fabricating freeze-resistant liquid-state energy storage are of two types. One method is increasing the solute concentration of aqueous electrolytes to lower the freezing point.[8] But such high-concentrated solutions of acid, alkali or salt would cause severe corrosion and side reactions, typically leading to the performance degradation and device failure.[9] The other approach is employing the organic electrolytes with a wide working temperature window.[10, 11] However, most non-aqueous electrolytes suffer from the toxicity and flammability issues, which require complicated and stringent fabrication processes.[12, 13] In fact, these are both passive strategies to fabricate anti-freezing hydrogel electrolytes. Achieving ideal anti-freezing hydrogel electrolyte requires the synergy of these physicochemical aspects fundamentally: (i) low freezing point, (ii) innocuous and harmless, (iii) superior ionic conductivity, (iv) excellent mechanical property. Hydrogel electrolytes satisfying these aspects are vital for anti-freezing aqueous flexible batteries, however, still in severe shortage, ascribing to the full complexity of material designing and synthesizing for the targeted electrolyte with extremely cold temperature tolerance.

Low molecular vicinal alcohols, such as glycerol and ethylene glycol (EG), are well-known nontoxic inhibitors for water freezing and have been widely used as engine coolant in industry.[14, 15] In these binary solutions, alcohols form stable molecular clusters with H_2O molecules that compete with hydrogen bonds in water, leading to a decrease of the saturated vapor pressure of water.[16] As a result, the formation of crystal lattices of ice is disrupted and the freezing point is decreased. However, owing to the low molecular weight and absence of double bonds, alcohols cannot be directly used to synthesize hydrogel matrix by conventional polymerization method. Although we can form hydrogels through copolymerizing acrylamide (AM) or acrylic acid (AA) monomers in EG-water binary solvent, the non-sacrificial hydrogen bonds between alcohol molecules and polymer chains are vulnerable to

[a] Department of Materials Science and Engineering, City University of Hong Kong, 83 Tat Chee Avenue, Kowloon, Hong Kong 999077, China. E-mail: cy.zhi@cityu.edu.hk
[b] Key Laboratory for Advanced Technology in Environmental Protection of Jiangsu Province, Yancheng Institute of Technology, Yancheng, Jiangsu 224051, China.
[c] Shenzhen Research Institute, City University of Hong Kong, Nanshan District, Shenzhen 518057, PR China.
† These authors contributed equally to this work.
Electronic Supplementary Information (ESI) available: [details of any supplementary information available should be included here]. See DOI: 10.1039/x0xx00000x

debonding under deformation, which do not have long-term stability. Moreover, the introduction of alcohols would further degenerate the intrinsically weak mechanical properties of physically cross-linked hydrogels. Therefore, it is of great importance to break the routine of classical hydrogel electrolytes which involve ordinary alcohols-water system.

Accordingly, the anti-freezing hydrogel electrolytes were designed on the basis of two criteria: (i) The alcohols molecules must be anchored onto the polymer chains through covalent bonds to form a stable unified matrix. (ii) To satisfy daily use of flexible and wearable batteries, the hydrogel matrix must be tough enough even at very low temperature while being compliant to mechanical impacts, including being folded, compressed, hammered, among others. To achieve the first criterion, we synthesized a series of EG based waterborne anionic polyurethane acrylates (EG-waPUA) by a step-growth polymerization,[17, 18] utilizing EG and isophorone diisocyanate (IPDI) as monomers, dimethylol propionic acid (DMPA) as chain extenders. Inside the polymeric matrix, the hydroxyl groups of EG molecules bind covalently with isocyanate groups, forming stable chemically anchor instead of simple hydrogen-bonding interactions in polymer chains. After adding hydroxyethyl methacrylate (HEMA) as end-capping regent, double bonds were introduced to terminate both sides of the polymer chains (Figure 1a). These double bond terminal groups are essential for free radical polymerization (FRP).[19] The second criterion is satisfied by copolymerizing EG-waPUA precursor and AM monomers through a FRP method to form a novel EG-waPUA/PAM based dual crosslinked hydrogel. In the geometric structure, the EG-waPUA polymer chains act as chemical covalent cross-linking points, significantly strengthening the network matrix. Moreover, sufficient hydrogen bonds form among the intra- and intermolecular of PAM polymer chains, which can dynamically homogenize the network and dissipate energy under deformation (Figure 1b).[20] This combination of covalent cross-linking bonding and physical hydrogen bonding endows the synthesized hydrogel with excellent flexibility and extensibility. Figure 1c presents the strong hydrogen-bonding interactions among water, EG-waPUA and PAM matrix, which firmly lock water molecules in the anti-freezing hydrogel (AF-gel). The anti-freezing mechanism will be discussed in depth later. The water contained in AF-gel can dissolve ions, making the synthesized polyelectrolyte serve as good ionic conductors.

Considering the safety and the biocompatibility issues of flexible and wearable batteries design, rechargeable aqueous zinc manganese-dioxide batteries (Zn-MnO_2-B) are particularly advantageous in virtue of inherent safety, negligible toxicity, and low flammability in comparing with traditional lithium ion batteries, and are thus selected as a mode system to demonstrate freeze-resistant aqueous batteries.[21-24]

In this paper, we introduce a novel flexible aqueous Zn-MnO_2-B that featuring freeze-tolerance down to -20 °C equipped with the designed EG-waPUA/PAM hydrogel electrolyte and an α-MnO_2/carbon nanotube (CNT) nanocomposites cathode. At normal temperature, the anti-freezing Zn-MnO_2-B (AF-battery) delivers a specific capacity of 275 mA h g^{-1} at the current density of 0.2 A g^{-1}, and a high volumetric energy density of 32.68 mW h cm^{-3}. Even at the extremely cold temperature of -20 °C, the AF-battery still delivers a high specific capacity of 226 mA h g^{-1} (over 82% of the normal-temperature one) at 0.2 A g^{-1}, and an excellent capacity retention approaching as high as 72.54% of the initial value after 600 cycles at 2.4 A g^{-1}, in complete contrast to the sharp performance failure of the Zn-MnO_2-B with traditional PAM-gel electrolyte (PAM-battery) due to the freezing of electrolyte. More remarkably, the solid-state AF-battery maintains remarkable flexibility and reliability under severe conditions at -20 °C. It can be bent, compressed, hammered and even washed in ice bath without packaging for almost 20 min. As an application demonstration, the aqueous AF-batteries were sealed into solid ice to power electronic watches, LED lights and electroluminescent panels, exhibiting great potential for wearable electronics in the extremely cold environment.

Formulation and Characterization of AF-Gel Electrolyte

With the use of these design principles, we synthesized a family of EG-waPUA/PAM hydrogel electrolytes according to the route outlined in Figure S1. ^{1}H-NMR and FT-IR were employed to confirm the molecular structure of EG-waPUA precursor end-capped with abundant end double bonds (Figure S2). This precursor exhibited excellent solubility so that it can serve as an ideal crosslinking agent for copolymerizing with the AM monomer. It should be noted that in order to introduce the multivalent cations such as Zn^{2+} and Mn^{2+} ions, the as-prepared EG-waPUA, ammonium persulphate (APS) and AM monomer were dissolved into a dispersion medium of 2 mol L^{-1} $ZnSO_4$ and 0.1 mol L^{-1} $MnSO_4$ mixture, followed by heat treatment at 60 °C to initiate the FRP reaction. The synthesized EG-waPUA/PAM hydrogel exhibits a transparent state, for easy observation we dyed it with a blue ink (Figure S3).

The EG-waPUA/PAM hydrogel exhibited exceptional mechanical performance, which was achieved by tuning the weight percentage of EG-waPUA (G_w%) in the hydrogel components. A specific G_w% improved the EG-waPUA/PAM hydrogel with optimized high stretchability and compressibility, remarkably outperforming the pure PAM-gel (Figure S4 and S5). In contrast, the PAM-EG hydrogels, which are formed in an EG/H_2O binary solution without covalent crosslinking, exhibited much poor extension properties. A possible explanation is that the non-sacrificial EG component cannot dissolve the AM monomers or form matrix network independently, thus retarding the polymerization of hydrogel. The strength enhancement of the EG-waPUA/PAM hydrogels is mainly attributed to the synergistic effects as below. First, the synthesized hydrogels are formed through covalent interactions of laterally associated EG-waPUA polymer chains

View Article Online
DOI: 10.1039/C8EE02892C

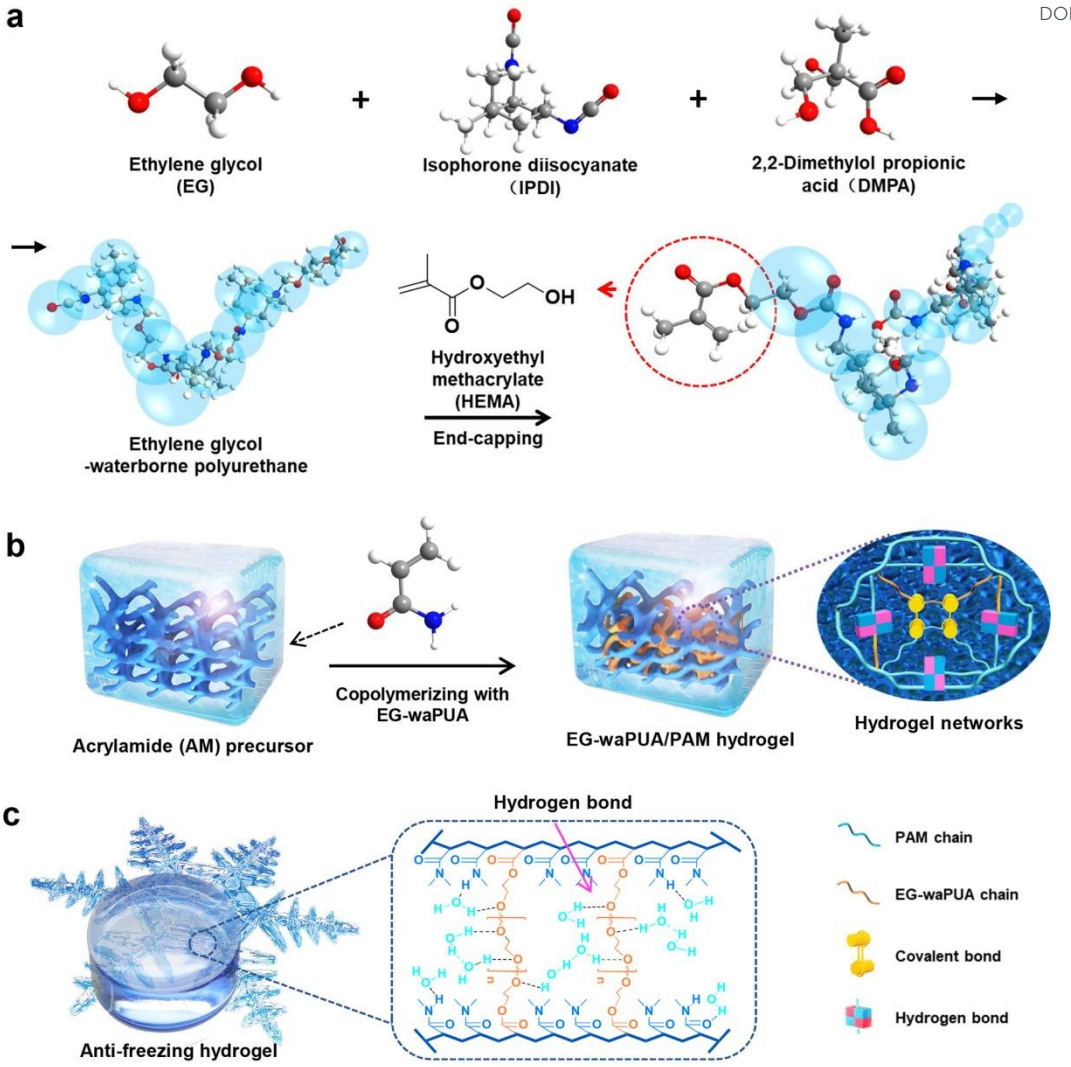

Figure 1. Design principles of the AF-gel electrolyte. (a) Schematic synthesis of the double bonds terminated EG-waPUA. (b) Polymerization of EG-waPUA and AM monomers to form the EG-waPUA/PAM hydrogel. The covalent/hydrogen hybrid crosslinked networks synergistically contributed to the excellent mechanical performance. (c) Schematic illustration of the strong hydrogen bonds between EG-waPUA, water and PAM in the AF-gel.

and physical entanglements of PAM polymer helices in extended junction zones (Figure 2a and S6). Second, the EG-waPUA chains were able to serve as stress buffers to dissipate energy, thus strengthening the network structure under deformation. Third, the PAM polymer chains provide sufficient intra-intermolecular hydrogen bonding, which can dynamically recombine to homogenize the network when the external force acts. Therefore, the dual crosslinked structure endows the hydrogels with excellent mechanical property.

The anti-freezing property of the EG-waPUA/PAM hydrogels was also highly dependent on the G_w%. As shown in Figure 2b, it is evident that the mixed solution of EG-waPUA/AM with G_w% exceeding 24% did not freeze at -20 °C. Correspondingly, the EG-waPUA/PAM hydrogels formed by using the EG-waPUA/AM precursor with G_w% over 24% well kept the states, whereas others were frozen into solid at -20 °C. In addition, upon cooling to -20 °C, the storage modulus (G') of the PAM-gel abruptly increased by almost 6×10^3 times (Figure 2c). At that temperature, the hydrogel turned into a fragile ice-like solid that could be easily broken. Alternatively, the G' of EG-waPUA/PAM hydrogels with 24% G_w% remained stable at the temperature range (30 to -20°C). As the temperature further decreased from -20 to -30 °C, the G' increased from 2.5×10^3 to 3.2×10^6 Pa with a reflection point at around -24 °C, corresponding to the crystalline peak in the differential scanning calorimetry (DSC) curve (Inset in the Figure 2c). For the hydrogel with higher G_w% of 40%, the G' maintained an almost constant during the temperature range (30 to -30 °C), showing the stable mechanical strength and elasticity due to the low freezing point. These results indicate that the hydrogel

View Article Online
DOI: 10.1039/C8EE02892C

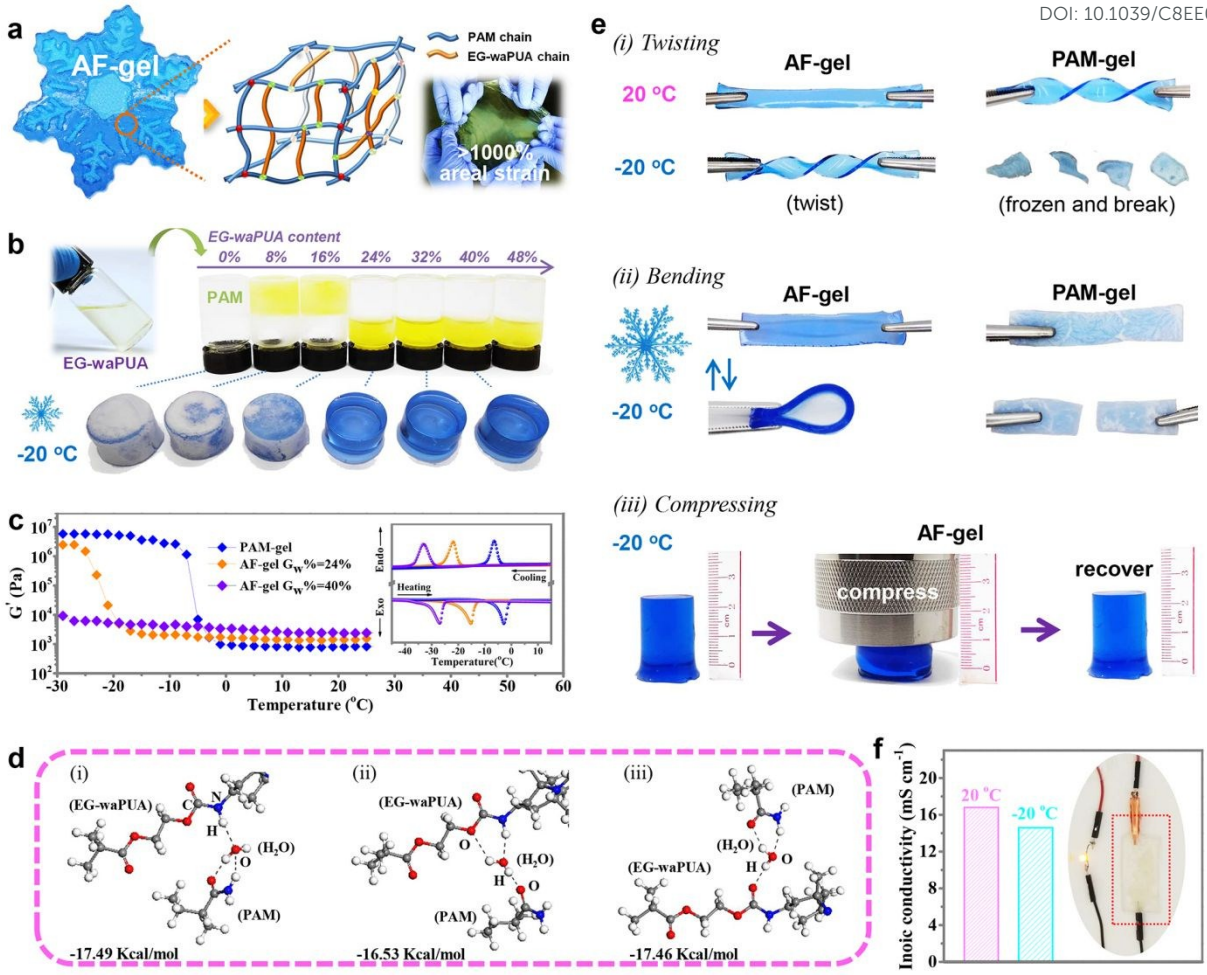

Figure 2. Characteristics of the AF-gel electrolyte. (a) Optical images of the AF-gel (colored blue for visibility) and a hypothetical molecular model. The soft hydrogel can be stretched more than 1000% in area without fracture. The dots with different colors indicate hydrogen bonds among different species (see Figure S6 for details) (b) The effect of EG-waPUA weight percentage (G_w%) on the freeze-resistant performance of the hydrogel electrolyte after one day of cooling at -20 °C. The EG-waPUA/water solutions were stained by yellow ink (0.1 wt%). (c) The storage modulus (G') of the PAM-gel, AF-gel with 24% G_w% and AF-gel with 40% G_w%. Inset is the corresponding DSC curves. (d) DFT analysis of water molecules, PAM, and EG-waPUA interacting with polymer chains *via* multiple hydrogen-bonding interactions in the AF-gel. (e) Elastic stability of AF-gel at -20 °C. i) twisted, ii) bent, and iii) compressed. (f) Ionic conductivity calculated from AC impedance spectra (Inset is an optical image showing an AF-gel film can serve as an ionic conductor to connect the LED circuit).

with different G_w% exhibited different working temperature range. The freezing point of the hydrogels could be controlled by tuning the EG-waPUA weight contents (G_w%) as shown in Figure S7. Specifically, the freezing-point of the EG-waPUA/PAM hydrogels with 24% G_w% approached approximately -25 °C. Hereafter, the as-prepared high G_w% hydrogels which can withstand the temperature of -20 °C is referred as AF-gel. As a proof concept, we selected the sample of EG-waPUA/PAM hydrogel with 24% G_w% as a model system to execute the electrochemical performance test.

To investigate the anti-freezing mechanism of the AF-gel, density functional theory (DFT) calculations were performed to calculate the interaction energy of hydrogen bonds between hydrogel chains and water molecules with Dmol^3/GGA-PBE/DNP basis set.[25-27] The results are shown in Figure S8-S10 and Table S1. We can observe that the interaction of EG and water (-5.27 Kcal/mol) is stronger than that of water-water (-3.83 Kcal/mol). When only one precursor presented, the binding energy of EG-waPUA-water and PAM-water is -6.7 Kcal/mol and -10.67 Kcal/mol, respectively, exceeding that of EG and water. When both EG-waPUA and PAM presented, there are three types of interaction among (EG-waPUA), PAM and water existing in the polymer matrix (Figure 2d and Figure S10) with the corresponding binding energies of (EG-waPUA)-PAM-Water ranging from -16.53 to -17.49 Kcal/mol. The interaction energy of the integral hydrogel networks to water molecules is thrice that of EG and water. The enhanced molecule interaction is ascribed to the synergistic effects as follow. First, water

View Article Online
DOI: 10.1039/C8EE03830

molecules provided enough interactions to enhance the interaction between EG-waPUA and PAM polymer chains. As shown in Figure S10, the water molecules, like a bridge, connect the hydroxyl groups of the EG-waPUA and the carbonyl groups of the PAM chains together, thus increased the binding energies. Second, the multiple interactions can firmly lock water molecules in the polymer networks and disrupt the formation of crystal lattices, endowing the AF-gel with excellent anti-freezing property.

After one day's storage at -20 °C, the mechanical properties of the AF-gels were well preserved, exhibiting high elasticity to sustain various large deformations including twisting, bending and compressing. Once the external force withdrew, quickly recovery occurred from deformed shapes, showing the high resilience of AF-gels at cold temperature of -20 °C (Figure 2e). In contrast, the PAM hydrogels were frozen into ice solid at -20 °C and broken when large twisting or bending is imposed. In addition, a scanning electron microscope (SEM) image of the freeze-dried AF-gel shows abundant micropores in the polymer matrix available for the transportation of zinc ions, enabling superior ionic conductivity (Figure S11). Moreover, the ionic conductivity of the AF-gel electrolyte containing 2 mol L^{-1} $ZnSO_4$ and 0.1 mol L^{-1} $MnSO_4$ was calculated to be 16.8 mS cm^{-1}, which was comparable to other zinc ion conducting polyelectrolytes in the literatures (Figure S12). Even at -20 °C it remained a high ionic conductivity of 14.6 mS cm^{-1}, certifying the stable ionic transportation at subzero temperatures (Figure 2f and S13). These results firmly validate the use of AF-gel as the electrolyte for freeze-resistant flexible Zn-MnO_2-B.

Fabrication and Electrochemical Performance of AF-battery

The cathode material, α-MnO_2/CNT composite, was synthesized by a hydrothermal and cop-precipitation method. The as-prepared homogeneous slurry was then blade-coated onto a piece of flexible CNT cloth substrate that featuring high conductivity (Figure S14 and S15a).[28] The flexible Zn anode was obtained by electroplating a uniform zinc film on the surface of the nickel-copper cloth (Figure S14). The continuous nickel-copper cloth, an assembly of interweaved nickel and copper silks, was an ideal material to deposit zinc film in virtue of its light weight, superior electrical conductivity and exceptional softness (Figure S15b).

The XRD pattern of the MnO_2/CNT composites, which exhibiting the crystalline phases, are well-indexed to the characteristic peaks of α-MnO_2 (JCPDS:44-0141), verifying the successful synthesis of α-MnO_2 (Figure S16).[29, 30] Transmission electron microscopy (TEM) image of α-MnO_2/CNT composite intuitively shows the morphology the MnO_2 nanorods with the diameter of 20-40 nm (Figure 3a). The high resolution TEM image manifests the homogeneous one-dimensional nanorod structure of α-MnO_2 with a lattice spacing of 0.685 nm for the (110) plane, confirming that the as-fabricated α-MnO_2 is highly crystalline (Figure 3b). Furthermore, the SEM image of the zinc anode as given in Figure 3c presents that the electroplated zinc on the nickel-copper cloth exhibits a unique flower-like nanosheet structure, which can possibly facilitate the interfacial compatibility of gel electrolyte/zinc anode and a fast charge transport.

To demonstrate the design of AF-battery, a piece of the as-synthesized AF-gel electrolyte, serving as the separator at the same time, was sandwiched between the fabricated flexible zinc anode and α-MnO_2/CNT cathode to assemble the free-standing full cell, as illustrated in Figure 3d. In virtue of both the soft and bendable electrodes, along with the high adhesion of AF-gel electrolyte avoiding exfoliation from the electrode surface, a flexible, quasi-solid state Zn-MnO_2-B was achieved (Figure S17). Initially, we measured the electrochemical performance of the fabricated Zn-MnO_2-B in normal condition (20 °C) (Figure S18), and corresponding electrochemical reaction mechanism was shown in Figure S19. The results indicate that the AF-battery can deliver a high capacity of 275 mA h g^{-1} at the current density of 0.2 A g^{-1} with a voltage of 1.8 V. Its highest volumetric energy density reached 32.68 mW h cm^{-3}, considerably overmatching some representative energy storage devices in the literatures (Figure S20). For comparing the freeze-resistant performances of the AF-battery, PAM-battery was also fabricated as the control group.

The temperature influence of the electrochemical properties of Zn-MnO_2-B was examined while the device was operated inside an ultra-low freezer. The comparing CV profiles of the PAM-battery and AF-battery recorded for several minutes at -20, -10, 0, 10 and 20 °C are shown in Figure 3e and 3f. When the temperature was decreased to -20 °C, the charge-discharge currents of the PAM-battery decreased significantly with the redox peaks even vanished below -10 °C, which resulted from the fact that the freezing of the electrolyte vastly inhibits the migration of zinc ions. On the other hand, for the AF-battery, all CV curves displayed distinguished redox peaks with almost equal peak intensity as well as negligible voltage polarization, manifesting the excellent reaction reversibility in cold conditions. Galvanostatic charge-discharge (GCD) curves at 0.2 A g^{-1} presents that the AF-battery delivered a specific capacity of 226 mA h g^{-1} at -20 °C (Figure 3h) on comparing with that of approximately 0 mA h g^{-1} of the PAM-battery (Figure 3g). The discharge capacity retentions of the AF-battery at 0 and -20 °C compared with that at 20 °C are 88.36 % (243 mA h g^{-1}) and 82.18 %, respectively. The volumetric energy density remained a high value of 26.22 mW h cm^{-3} at -20 °C, nearly three times higher than that of the reported NiCo//Zn textile batteries (8 mW h cm^{-3}) and Ni-Zn batteries (7.76 mW h cm^{-3}) (Figure S20).[31, 32] The extraordinary temperature stability was also observed for energy density and power density, as shown in the Ragone plot based on the weight of cathode material of AF-battery (Figure S21). In addition, the discharging curves of AF-battery show almost overlapped plateaus in the voltage range of 1.3-1.7 V, but separated from 1.3 to 0.9 V at different testing temperatures. A possible explanation is that for the aqueous Zn-MnO_2-B, the first discharging plateaus (1.3-1.7 V) is mainly ascribed to the H^+ insertion into the cathode material (MnO_2), whereas the second voltage plateau from 1.3-0.9 V is derived from the Zn^{2+} insertion and formation of zinc hydroxide sulfate.

The reaction kinetics of first discharging plateau is much faster than that of second one.[22] Benefitting from the outstanding stability of conductivity of our AF-gel electrolyte at -20 °C, the proton insertion at voltage range of 1.3-1.7 V would not be influenced that the discharging curves overlapped. But for the second plateau, the discharge curves at different temperature separated probably owing to the lightly retarded behaviour of Zn^{2+} insertion kinetics and formation of zinc hydroxide sulfate at low temperature. Electrochemical impedance spectroscopy (EIS) plots of the Zn-MnO_2-Bs were also recorded at 20, 0 and -20 °C (Figure 3i and 3j). Moreover, as exhibited in Figure S22, EIS can be fitted by an equivalent circuit shown in inset of Figure S22. Upon cooling from 20 to -20 °C, the faradic charge-transfer resistance (R_{ct}) for the PAM-battery considerably increased from 160.3 Ω to 7759 Ω due to the freezing of electrolyte, along with the increased interface resistance (R_i) from 18.02 Ω to 366 Ω. On the other hand, the R_{ct} of AF-battery only increased from 221.8 Ω to 476.5 Ω, with a slight increase of R_i from 19.07 Ω to 31.05 Ω, outperforming the comparison PAM-battery. This well-maintained ion conductivity at -20 °C is intrinsically ascribed to the low-temperature durability and the high compatibility with electrodes of AF-gel electrolyte (Figure S23). These results demonstrate that the AF-battery can withstand low temperature down to -20 °C.

We further evaluated the cold tolerance regarding the charge/discharge stability of the electrolytes. As shown in

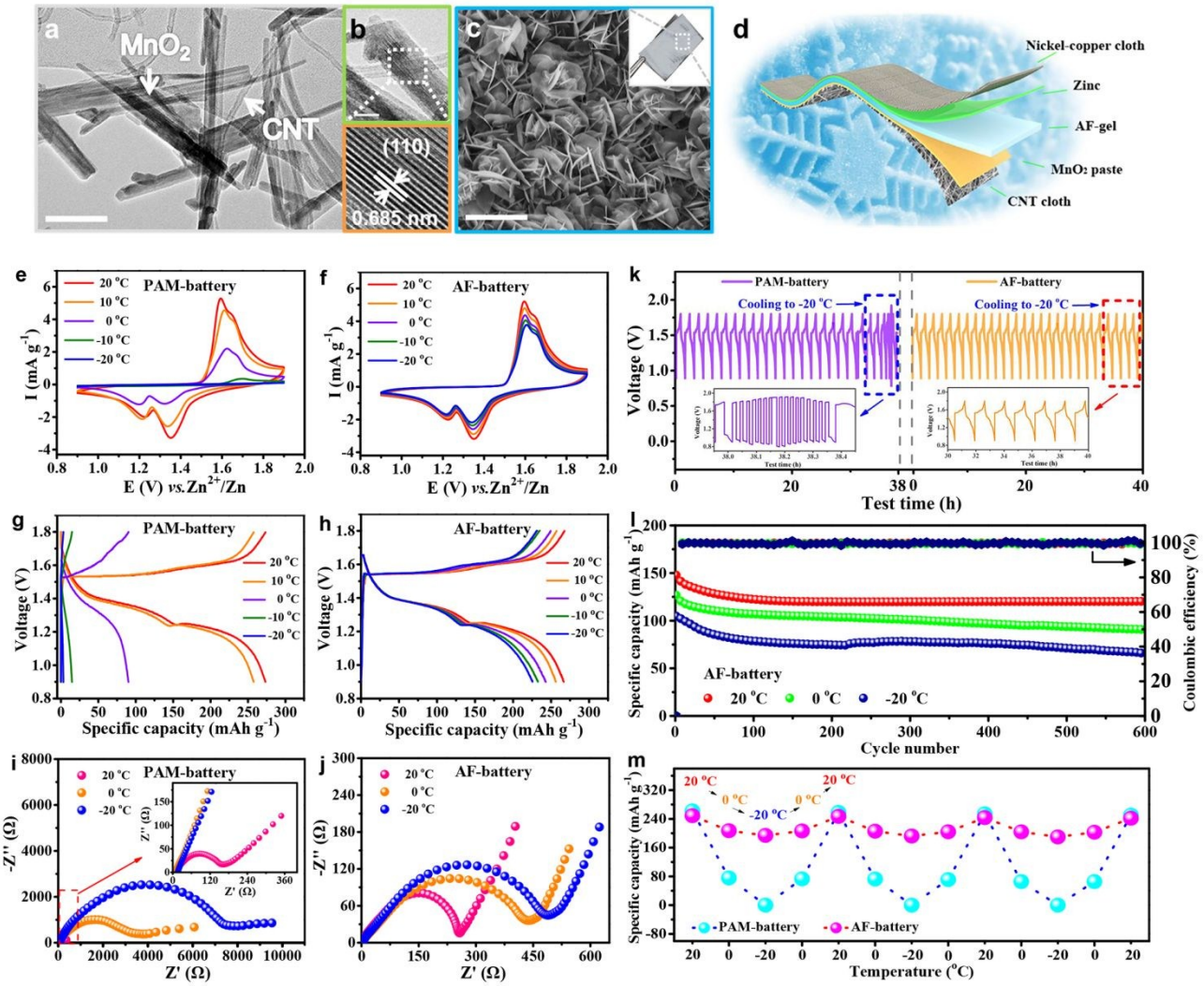

Figure 3. AF-battery assembly and electrochemical performance of batteries over the temperature range from -20 to 20 °C. (a) TEM image of the α-MnO_2/CNT composites. (b) HRTEM image of the α-MnO_2/CNT composites. The inset indicates lattice fringes along (110) plane. (c) SEM image of the zinc anode. The inset is a photograph of flexible zinc anode. Scale bars: (a) 200 nm, (b) 20 nm, (c) 2 µm. (d) Schematic illustration of the structure of AF-battery. CV profiles of (e) PAM-battery and (f) AF-battery at the scan rate of 2 mV s^{-1}. GCD curves of (g) PAM-battery and (h) AF-battery at the current density of 0.2 A g^{-1}. Impedance spectra of (i) PAM-battery and (j) AF-battery recorded at 20, 0, -20 °C. (k) Voltage profiles of PAM-battery and AF-battery along with cyclic cooling and heating process at 0.8 A g^{-1}. (l) Extended cycling performance at 2.4 A g^{-1} of the AF-battery at different temperatures. (m) Cyclic testing of PAM-battery and AF-battery under 20, 0, -20 °C at 0.3 A g^{-1}.

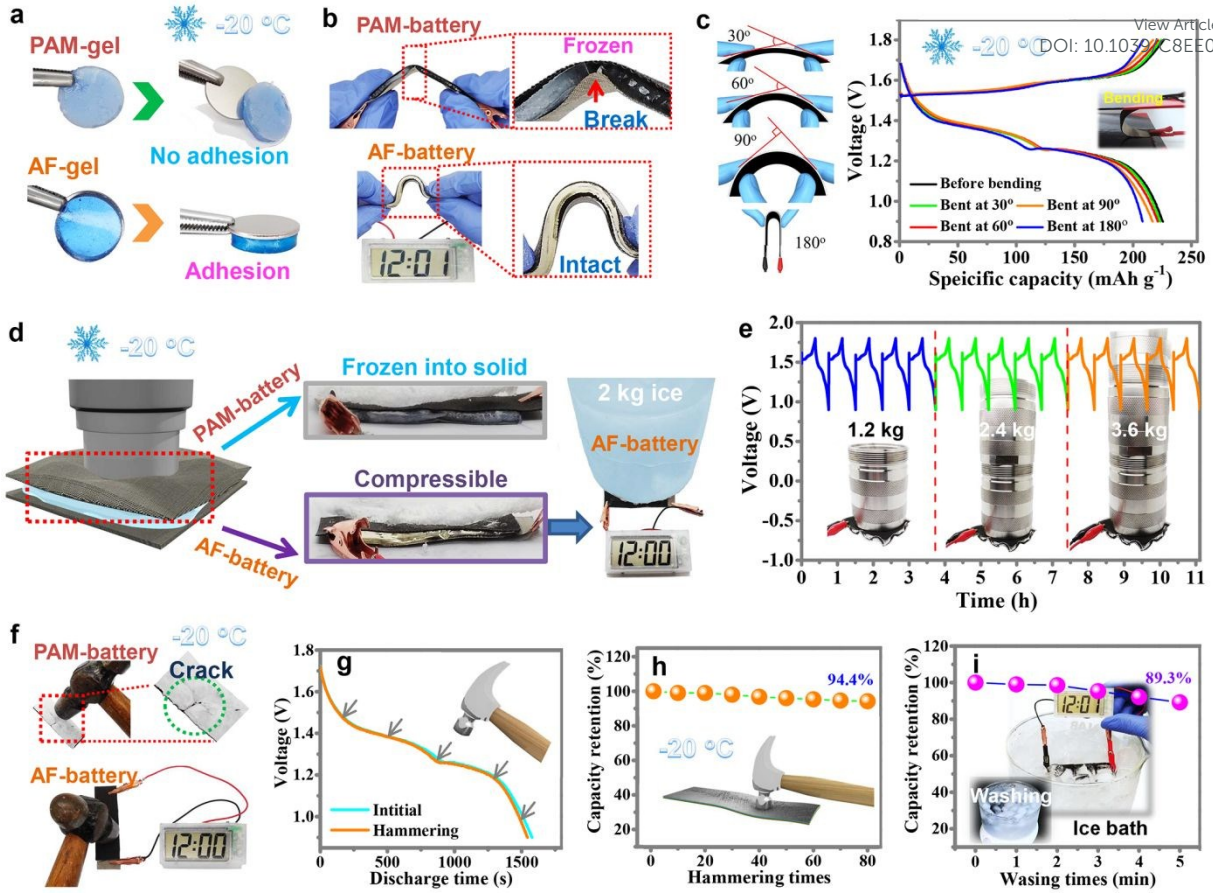

Figure 4. Electrochemical performance of AF-battery in various destructive experiments at subzero temperatures. (a) Comparisons of adhesion force of PAM-gel and AF-gel at -20 °C. (b) Demonstration of bending the PAM-battery and AF-battery at -20 °C. (c) Illustration of bending AF-battery at different angles and the corresponding GCD curves at 0.2 A g^{-1}. (d) Photographs of PAM-battery and AF-battery holding an approximately 2.0 kg ice block (134-fold weight heavy loads of the batteries) at -20 °C, the AF-battery was capable to power an electrical watch. (e) GCD cycling curves of AF-battery at a current density of 0.6 A g^{-1} undergoing various heavy loads -20 °C. (f) Consecutive hammering tests of PAM-battery and AF-battery after one day of cooling at -20 °C and (g) the corresponding discharge curves of AF-battery. (h) Capacity retention of AF-battery in hammering test measured at -20 °C. (i) Capacity retention of AF-battery in washing test in an ice bath.

Figure 3k, the AF-battery showed a stable rechargeability without any obvious voltage change upon cooling, whereas the comparison PAM-battery exhibited notably large augment of the voltage hysteresis, especially when the temperature decreased to -20 °C. For cycling performance, the AF-battery delivered a capacity of 146 mA h g^{-1} at 2.4 A g^{-1} with a retention of 87.41% of its initial capacity after 600 cycles at 20 °C (Figure 3l). Furthermore, a high cycling stability to temperature is also manifested for the AF-battery with 81.67% (0 °C) and 74.54 % (-20 °C) capacity retentions over 600 cycles at 2.4 A g^{-1}, respectively. The Coulombic efficiencies of the AF-battery remain as high as approximately 100% even at -20 °C. Experimental results of the AF-battery and PAM-battery cycled sequentially at 20, 0 and -20 °C are shown in Figure 3m. For the PAM-battery, a degraded capacity upon cooling is obtained in a way that the battery retains only 27.44% at 0 °C and 0.01% at -20 °C. In contrast, the AF-battery delivered a high capacity of 244 mA h g^{-1} at 0.3 A g^{-1} at 20 °C. When the temperature dropped from 20 °C to 0 °C and -20 °C, the capacities at low temperature are 85.78% (209 mA h g^{-1} at 0 °C) and 80.67% (196 mA h g^{-1} at -20 °C) of that delivered at 20 °C. While the temperature increased back to 0 °C and 20 °C, the specific capacity of the AF-battery almost restored to the pristine one. After multiple cycles of cooling-heating-cooling process, no significant capacity attenuation could be identified, guaranteeing its practical application.

Flexible AF-battery at Subzero Temperatures

Benefitting from the flexible components (AF-gel, carbon cloth, and nickel-copper cloth), the capacity retention of the flexible AF-battery could remain over 96 % under various deformations (Figure S24) at room temperature and was capable to continually power an electronic watch even being heavily deformed. To evaluate whether the flexible Zn-MnO_2-B can operate well in extremely cold condition, the batteries were subjected to a series of mechanical tests including bending, compressing, hammering at -20 °C and washing in ice bath.

First, note that the hard and brittle surface of the freezing

View Article Online
DOI: 10.1039/C8EE02892C

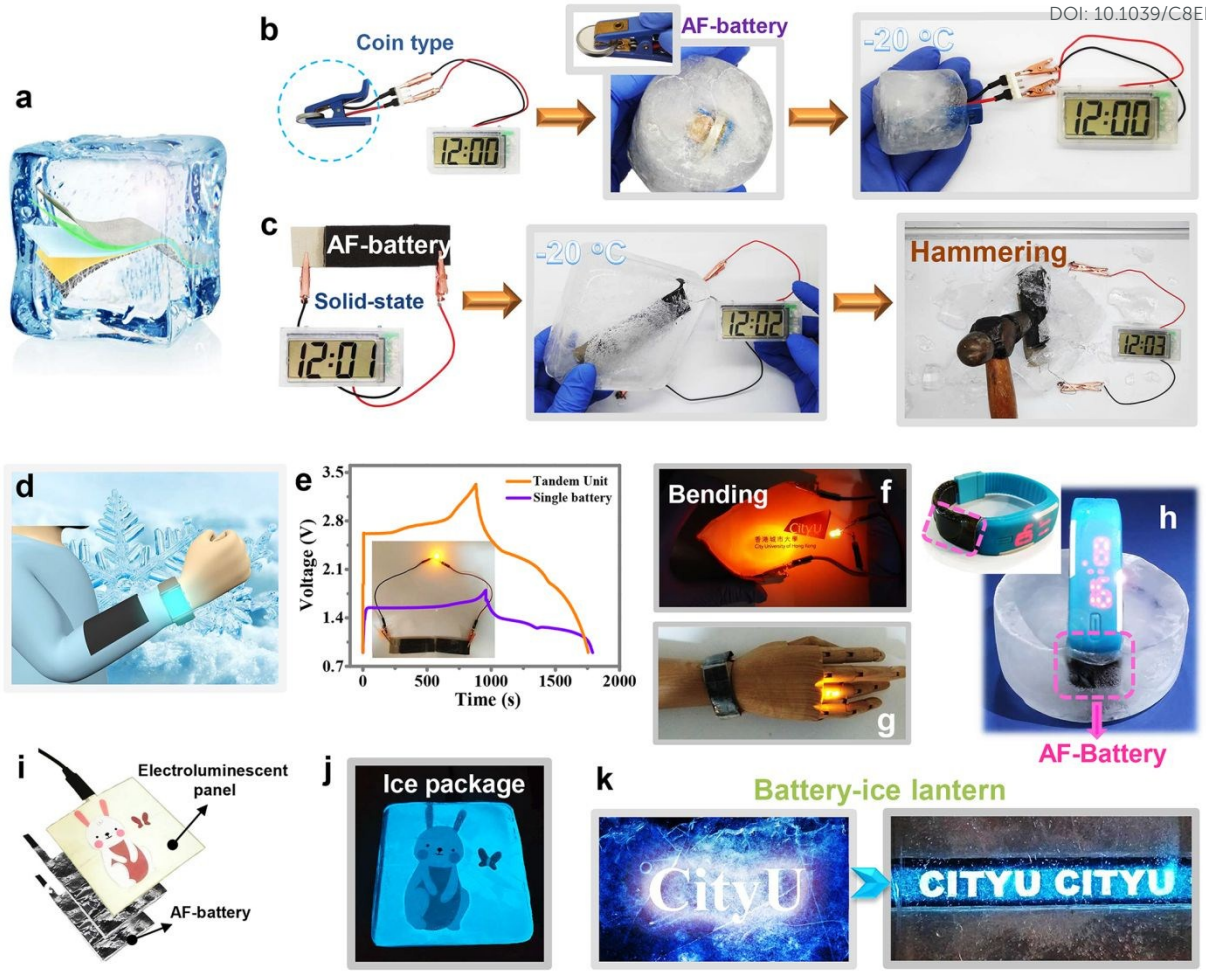

Figure 5. Applications demonstration of AF-battery at subzero temperatures. (a) Schematic illustration of the AF-battery in ice package. Freeze-resistant performance of the (b) coin-type and (c) solid-state flexible AF-batteries. (d) Schematic illustration of AF-battery powering wearable electronics at subzero temperature. (e) GCD curves of the two AF-batteries connected in series. Inset is an optical image of the tandem unit to power a yellow LED (1.8 V voltage needed). (f)-(g) Photographs of the tandem unit under a bending state and mounted on the demonstrator's wrist, powering a yellow LED in a -20 °C cryogenic box. (h) Two AF-batteries were connected in series to operate a wristband electrical watch while being sealed into ice solid. (i-k) two planar batteries connected in series to power various electroluminescent panels. The whole circuits were encapsulated in ice.

hydrogel would inevitably decrease the adhesion of electrode-electrolyte interface, leading to high interfacial resistance. Figure 4a illustrates that the AF-gel can maintain high adhesiveness at -20 °C, which was attributed to the presence of EG-waPUA and PAM chains synergistically locking water molecules and lowing the vapor pressure. After being decreased to the temperature of -20 °C, the flexible AF-battery still exhibited superior mechanical property instead of turning into an ice-like solid, and no interfacial void space was detected under regular bending (Figure 4b). As a further demonstration, the AF-battery was fixed at various bending states (30°, 60°, 90° and 180°) and the corresponding GCD curves are shown in Figure 4c and S25. It is observed that the charge-discharge voltage plateaus are all at around 1.6 V and 1.35 V respectively, and the plateaus exhibited only subtle vibration associated with minor capacity change. Furthermore, SEM was performed to characterize the morphological structure of electrodes and electrolyte of AF-battery after 500 bending cycles and 500 twisting cycles, respectively. The results illustrated that no appreciable mechanical cracks and sharp creases could be detected on all the three layers of the AF-battery (see from top view), indicating the excellent mechanical stability of our devices after cycling deformation (Figure S26).

The rechargeable characteristic of the AF-battery under different compressions at -20 °C is also investigated through conducting five charge-discharge cycles at each strain at 0.6 A g^{-1} (Figure 4d and 4e). It was capable to bear 3.6 kg (approximately 240-fold weight heavy loads of the battery) with around 50% compression correspondingly. More importantly, the charge-discharge characteristics could be well maintained

without appreciable changes, indicating dramatic charge-discharge capability in harsh condition.

To investigate the impact resistance of the solid-state AF-battery at extremely cold temperature, which is vital for whole device application, the Zn-MnO_2-Bs were subjected to consecutive hammering test after a day's storage at -20 °C. It could be observed that after being instantaneously hammered 5 times, the PAM-gel electrolyte in PAM-battery began to crack throughout the creases, resulting in the exfoliation of electrode. In contrast, the AF-battery could still work without fracture and continuously power an electronic watch (Figure 4f). The corresponding discharge characteristics were well maintained with only subtle changes (Figure 4g). In addition, no evident deterioration in capacity was detected even after eighty violent hammer strikes (Figure 4h), further demonstrating the excellent durability.

Moreover, the unpackaged AF-battery was immersed in an ice bath in a glass vessel and stirred continuously with a high power magnetic stirrer to simulate washing. As depicted in Figure 4i, the capacity retention of AF-battery approached 89.3% of its initial capacity after vigorous stirring for 5 min and the battery was still capable to power an electronic watch after stirring for over 20 min, certifying an impressive waterproof performance even without extra packaging. These results firmly confirmed both mechanical and electrochemical robustness of AF-battery in extremely cold conditions.

Applications of the AF-battery at Subzero Temperatures

To further verify the anti-freezing performances, a coin-type AF-battery was immersed in water in a glass vessel and placed at -20 °C to form an ice solid (Figure 5a and 5b). It could be observed that this "solid ice" battery was capable to continuously power the electronic watch (Movie S1) and 88.72% capacity was retained after 72 h's storage at -20 °C (Figure S27). Moreover, with excellent waterproof property and mechanical stability, an unpackaged solid-state AF-battery was also sealed into a solid ice. As depicted in Figure 5c, the battery sealed in ice could still work without failure (Movie S2) and power the electronic watch even after being violently hammer strikes until the ice was smashed (Movie S3).

To exemplify the viability for wearable applications in extremely cold condition, our flexible AF-battery was tested in various situations mimicking real usage (Figure 5d-h). With impressive mechanical durability and softness, the AF-batteries can be easily integrated in series to realize the device scalability. In comparison with a single battery with a peak voltage of 1.8 V, two tandem units of AF-batteries achieved an operating voltage of 3.6 V with a similar discharge time of single cells, which was high enough to power a yellow LED at repetitive deformations. More specially, the flexible AF-battery enables to work as a power source of a wristband of electronic watch under bent condition (Figure 5h). Even sealed the wristband-battery in ice solid, the device can be well operated without exceptions. Furthermore, two planar AF-batteries connected in series could power a 72 cm^2 electroluminescent panel (size 8 × 9 cm) *via* a current inverter, which could invert the direct current (DC) to alternating current (AC). Even encapsulating the whole circuit into ice in cold conditions, the AF-battery maintained a stable energy output for the electroluminescent panels (Figure 5i-k), confirming the feasibility of the whole device to serve as backlight sources for ice sculptures.

Considering the human living environment and practical applications of flexible aqueous batteries, -20 °C is a fairly low temperature, which far below the water-freezing temperature. The afore-demonstrated anti-freezing hydrogel electrolyte firmly validates their tremendous practical value as intrinsically freeze-tolerant aqueous battery, which can serve as a reliable and powerful energy storage device for various wearable electronics in extremely cold environment. Moreover, the electrochemical performance of AF-battery at normal and subzero temperatures was repeatability (Figure S28). Apart from freeze-resistance, anti-heating property is another research hotspot for hydrogel electrolyte based wearable batteries. Accordingly, the real-time influence of high temperature for the AF-batteries was also investigated under the temperature ranging from 20 to 80 °C (Figure S29). During the test, the battery was sealed inside a plastic bag to prevent the hydrogel electrolyte from dehydration. The results indicated that the AF-battery exhibited distinguished reduction/oxidation peaks in CV curves and delivered a higher specific capacity as the temperature increased. The enhanced battery performance was attributed to the faster ion transport at high temperature.

Conclusions

To conclude, we successfully fabricated an anti-freezing aqueous solid-state Zn-MnO_2 battery equipped with a novel designed EG-waPUA/PAM hydrogel electrolyte. Inside the polymer matrix, the strong cooperative hydrogen bonding with water firmly anchored the water molecules, thus endowing the hydrogel with impressive freeze-resistance and long-term stability even when the temperature fell down to -20 °C. The dual crosslinked structure is beneficial to the mechanical robustness, which could not be achieved by the hydrogels based on the EG-PAM mixed precursor. The sold-state AF-battery exhibits a high volumetric energy density of 32.68 mW h cm^{-3}, as well as a specific capacity of 275 mA h g^{-1} at 20 °C. Significantly, the discharge capacity retentions of the AF-battery at 0 and -20 °C compared with that at 20 °C are 88.36% (243 mA h g^{-1}) and 82.18% (226 mA h g^{-1}) at 0.2 A g^{-1} with high cycling stability of 81.67% (0 °C) and 74.54% (-20 °C) capacity retentions over 600 cycles at 2.4 A g^{-1}, respectively. Moreover, this AF-battery exhibits exceptional flexibility and durability in adverse mechanical environments, such as being bent, compressed, hammered at -20 °C and washed in ice bath, enabling a satisfactory level of architectural durability in extremely cold conditions. The combination of freeze-tolerance, excellent mechanical properties and high electrochemical performance

enable our AF-batteries to serve as reliable aqueous flexible batteries for wearable applications in harsh environments.

Conflicts of interest

There are no conflicts to declare.

Acknowledgements

This research was supported by GRF under Project CityU 11305218 and the work was also partially sponsored by the Science Technology and Innovation Committee of Shenzhen Municipality (the Grant No. JCYJ20170818103435068).

Notes and references

1 Y. Xu, Y. Zhang, Z. Guo, J. Ren, Y. Wang and H. Peng, *Angew. Chem. Int. Ed.*, 2015, **54**, 15610-15614.
2 T. Hazama, K. Fujii, T. Sakai, M. Aoki, H. Mimura, H. Eguchi, Y. Todorov, N. Yoshimoto and M. Morita, *J. Power Sources*, 2015, **286**, 470-474.
3 J. Zhao, K. K. Sonigara, J. Li, J. Zhang, B. Chen, J. Zhang, S. S. Soni, X. Zhou, G. Cui and L. Chen, *Angew. Chem. Int. Ed.*, 2017, **129**, 7979-7983
4 Q. Tang, M. Chen, G. Wang, H. Bao and P. Sáha, *J. Power Sources*, 2015, **284**, 400-408.
5 J. Bae, Y. Li, J. Zhang, X. Zhou, F. Zhao, Y. Shi, J. Goodenough and G. Yu, *Angew. Chem. Int. Ed.*, 2018, **57**, 2096-2100.
6 L. Ma, S. Chen, Z. Pei, H. Li, Z. Wang, Z. Liu, Z. Tang, J. A. Zapien and C. Zhi, *ACS nano*, 2018, **12**, 8597-8605.
7 H. Gao, Z. Zhao, Y. Cai, J. Zhou, W. Hua, L. Chen, L. Wang, J. Zhang, D. Han and M. Liu, *Nat. Commun.*, 2017, **8**, 15911.
8 T. Deng, W. Zhang, H. Zhang and W. Zheng, *Energy Technology*, 2018, **6**, 605-612.
9 D. W. McOwen, D. M. Seo, O. Borodin, J. Vatamanu, P. D. Boyle and W. A. Henderson, *Energ. Environ. Sci.*, 2014, **7**, 416-426.
10 Y. You, H. R. Yao, S. Xin, Y. X. Yin, T. T. Zuo, C. P. Yang, Y. G. Guo, Y. Cui, L. J. Wan and J. B. Goodenough, *Adv. Mater.*, 2016, **28**, 7243-7248.
11 X. Zang, R. Zhang, Z. Zhen, W. Lai, C. Yang, F. Kang and H. Zhu, *Nano Energy*, 2017, **40**, 224-232.
12 A. Manthiram, *ACS Central Sci.*, 2017, **3**, 1063-1069.
13 M. Zhu, Z. Wang, H. Li, Y. Xiong, Z. Liu, Z. Tang, Y. Huang, A. L. Rogach and C. Zhi, *Energ. Environ. Sci.*, 2018, DOI:10.1039/C8EE00590G.
14 W. P. Williams, P. J. Quinn, L. I. Tsonev and R. D. Koynova, *BBA-Biomembranes*, 1991, **1062**, 123-132.
15 S. Peyghambarzadeh, S. Hashemabadi, S. Hoseini and M. S. Jamnani, *Int. Commun. Heat Mass*, 2011, **38**, 1283-1290.
16 R. M. Kumar, P. Baskar, K. Balamurugan, S. Das and V. Subramanian, *J. Phys. Chem. A*, 2012, **116**, 4239-4247.
17 S. Koltzenburg, M. Maskos and O. Nuyken, *Polym. Chem.*, 2017, 163-204.
18 A. Santamaria-Echart, I. Fernandes, F. Barreiro, A. Retegi, A. Arbelaiz, M. A. Corcuera and A. Eceiza, *Prog. Org. Coat.*, 2018, **117**, 76-90.
19 H. Tobita and A. Hamielec, *Macromolecules*, 1989, **22**, 3098-3105.
20 X. Hu, M. Vatankhah-Varnoosfaderani, J. Zhou, Q. Li and S. S. Sheiko, *Adv. Mater.*, 2015, **27**, 6899-6905.
21 C. Xu, B. Li, H. Du and F. Kang, *Angew. Chem. Int. Ed.*, 2012, **51**, 933-935.
22 H. Pan, Y. Shao, P. Yan, Y. Cheng, K. S. Han, Z. Nie, C. Wang, J. Yang, X. Li, P. Bhattacharya, K. Mueller and J. Liu, *Nat. Energy*, 2016, **1**, 16039.
23 B. Lee, C. S. Yoon, H. R. Lee, K. Y. Chung, B. W. Cho and S. H. Oh, *Sci. Rep.*, 2014, **4**, 6066.
24 H. Li, Z. Liu, G. Liang, Y. Huang, Y. Huang, M. Zhu, Z. Pei, Q. Xue, Z. Tang, Y. Wang, B. Li and C. Zhi, *ACS nano*, 2018, **12**, 3140-3148.
25 J. Ireta, J. Neugebauer and M. Scheffler, *J. Phys. Chem A*, 2004, **108**, 5692-5698.
26 L. Han, K. Liu, M. Wang, K. Wang, L. Fang, H. Chen, J. Zhou and X. Lu, *Adv. Funct. Mater.*, 2018, **28**, 1704195.
27 A. D. Boese, *ChemPhysChem*, 2015, **16**, 978-985.
28 G. Xu, C. Zheng, Q. Zhang, J. Huang, M. Zhao, J. Nie, X. Wang and F. Wei, *Nano Res.*, 2011, **4**, 870-881.
29 H. Li, C. Han, Y. Huang, Y. Huang, M. Zhu, Z. Pei, Q. Xue, Z. Wang, Z. Liu and Z. Tang, *Energ. Environ. Sci.*, 2018, **11**, 941-951.
30 D. Xu, B. Li, C. Wei, Y. B. He, H. Du, X. Chu, X. Qin, Q.-H. Yang and F. Kang, *Electrochim. Acta*, 2014, **133**, 254-261.
31 Y. Huang, W. S. Ip, Y. Y. Lau, J. Sun, J. Zeng, N. S. S. Yeung, W. S. Ng, H. Li, Z. Pei, Q. Xue, Y. Wang, J. Yu, H. Hu and C. Zhi, *ACS nano*, 2017, **11**, 8953-8961.
32 J. Liu, C. Guan, C. Zhou, Z. Fan, Q. Ke, G. Zhang, C. Liu and J. Wang, *Adv. Mater.*, 2016, **28**, 8732-8739.

View Article Online
DOI: 10.1039/C8EE02892C

Broader context

The increasing popularity of portable and wearable electronics has boosted the development of flexible battery devices based on hydrogel electrolytes. However, one challenge identified in this field is how to surmount the freezing phenomena of these water-based hydrogel electrolytes as well as the maintenance of ionic conductivity and mechanical properties while working below water-freezing temperature. This work introduces a flexible rechargeable aqueous zinc manganese-dioxide battery based on an elaborately designed anti-freezing hydrogel polyelectrolyte that can work even at -20 °C. This freeze-resistant battery exhibits excellent energy-power density, stable cycling performance and remarkable flexibility at subzero temperatures, benefitting from the exceptional physicochemical properties of the anti-freezing hydrogel electrolyte. More importantly, the flexible battery also presents exceptional mechanical durability in adverse mechanical conditions, such as being bent, compressed, hammered, sealed in ice solid at -20 °C and washed in ice bath without packaging, which enabling a satisfactory level of architectural durability in extremely cold conditions. This research provides new insights in developing anti-freezing water-based electrolytes and shows great potential applications in wearable electronics in extremely cold regions.